

CFD ANALYSIS OF THE MATIS-H EXPERIMENTS ON THE TURBULENT FLOW STRUCTURES IN A 5x5 ROD BUNDLE WITH MIXING DEVICES

Hyung Seok KANG, Seok Kyu CHANG and Chul-Hwa SONG *

KAERI, Daedeok-daero 1045, Yuseong-gu, Daejeon 305-353, Republic of Korea

* E-mail: chsong@kaeri.re.kr

Abstract

The measurements of a turbulent swirl flow in the subchannels of a 5 x 5 rod array having typical mixing devices at the MATIS-H (Measurements and Analysis of Turbulence In Subchannels-Horizontal) facility have been analysed using a commercial CFD code of STAR-CCM+ 4.02 with a unit grid model having no unmatched grid interface. The main objectives of this analysis is to establish a proper CFD analysis methodology to this kind of very complicated turbulent swirling flow in a subchannel since previous results show that a predicted turbulent swirl flow within 5 times of hydraulic diameter length from the mixing devices tip shows different results, which are dependent on the models chosen, such as the turbulent model, wall function model, the y^+ value, and the numerical model for a convection term. In the MATIS-H experiment, the intrinsic features of turbulent flow along the elevation, which shows distinct characteristics very sensitively by depending on the types of the mixing devices (split and swirl types), were measured by 2-D LDA (Laser Doppler Anemometry) at the condition of $Re=48,000$ in the water loop being operated at 35°C and 1.5bar. A series of sensitivity analyses shows that a very dense mesh distribution along the stream-wise direction around the mixing devices is recommended to use for resolving a drastic change of the turbulent intensity due to a strong swirl flow induced by the mixing devices. And it is also shown that a non-linear or second-order closure model is required to adopt for properly predicting the anisotropic characteristics of the turbulent flow structures caused by the mixing devices in the sub-channel.

1. INTRODUCTION

A spacer grid that fixes the rods in a fuel assembly of nuclear reactor core has been used as an effective thermal mixing device by attaching various types of flow deflectors (Chang et al., 2008; Seo, 2009). Several types of mixing devices are currently being designed to develop an optimum spacer grid which can mix the flow effectively in the sub-channel of rod bundle geometry. The performance of mixing devices was previously examined by investigating a detailed flow structure of swirl flow and an enhancement of heat transfer coefficient due to the swirl flow mostly through an experimental work. In the experimental work, a LDA (Laser Doppler Anemometry) or PIV (Particle Image Velocimetry) was in general used to measure a vector profile and turbulent intensity in the sub-channel (Chang et al., 2008; Seo, 2009). However, the experimental work requires a lot of efforts to get reliable data because the LDV and PIV should be carefully and precisely operated in measuring the data in the flow channel.

The previous CFD analysis, introduced in the development of mixing devices for predicting the detailed flow structure and heat transfer phenomena in a sub-channel, showed that a predicted turbulent swirl flow within the distance of 5 times of hydraulic diameter from the mixing devices tip shows different results depending on the models chosen, such as the turbulent model, wall function model, the y^+ value, and the numerical model for a convection term (Kang et al., 2006; Kang & Song, 2008). Therefore, the development of general BPG (Best Practice Guidelines) to a simulation of the turbulent swirl flow due to the mixing devices in a rod bundle geometry is strongly recommended to set up for increasing the reliability of CFD analysis results (Mahaffy, 2010). In order to do so, a series of sensitivity analyses for the flow mixing tests at the MATIS-H facility with both the split and swirl type vanes has been performed using a commercial CFD code of STAR-CCM+ 4.02 by varying a grid cell distribution and a turbulent model including a nonlinear model, a wall function model and a

numerical model for a convection term. This analysis has mainly been made with the motivation that a validated CFD analysis methodology may be used as a basic step to reduce a DNB (Departure from Nucleate Boiling) margin in the core thermal hydraulic design (Bestion, 2010).

2. EXPERIMENTS

An experiment has been conducted in the water circulation loop, as shown in Fig. 1, at KAERI (Korea Atomic Energy Research Institute) that can perform the hydraulic test at the ambient pressure and temperature conditions for a rod bundle array (Chang et al., 2008). For a close examination of the lateral flow structure on sub-channel geometry, a 5x5 rod bundle array has been fabricated as 2.6 times larger than the prototypic size of PWR fuel bundles. The total channel length and the grid span are 4,900 mm and 1,700 mm, respectively. A 2-D LDA was used to measure the turbulent velocities in a rod bundle. The 2-D LDA was positioned in front of the main flow cross section of the 5x5 rod bundle array for measuring the lateral velocity vectors on every point in a flow sub-channel (Fig. 1). The axial velocity component was also measured by changing the location of the LDA probe to the side of the test section. The size of the inner square of the test section is 170x170 mm. The geometric configurations of the bundle array are: rod diameter of $D = 25.4$ mm, rod pitch of $P = 33.12$ mm and wall pitch of $S = 18.76$ mm, respectively. The measuring points were closely distributed with resolutions of 0.75 mm for precise examination of the lateral flow distribution in the sub-channels.

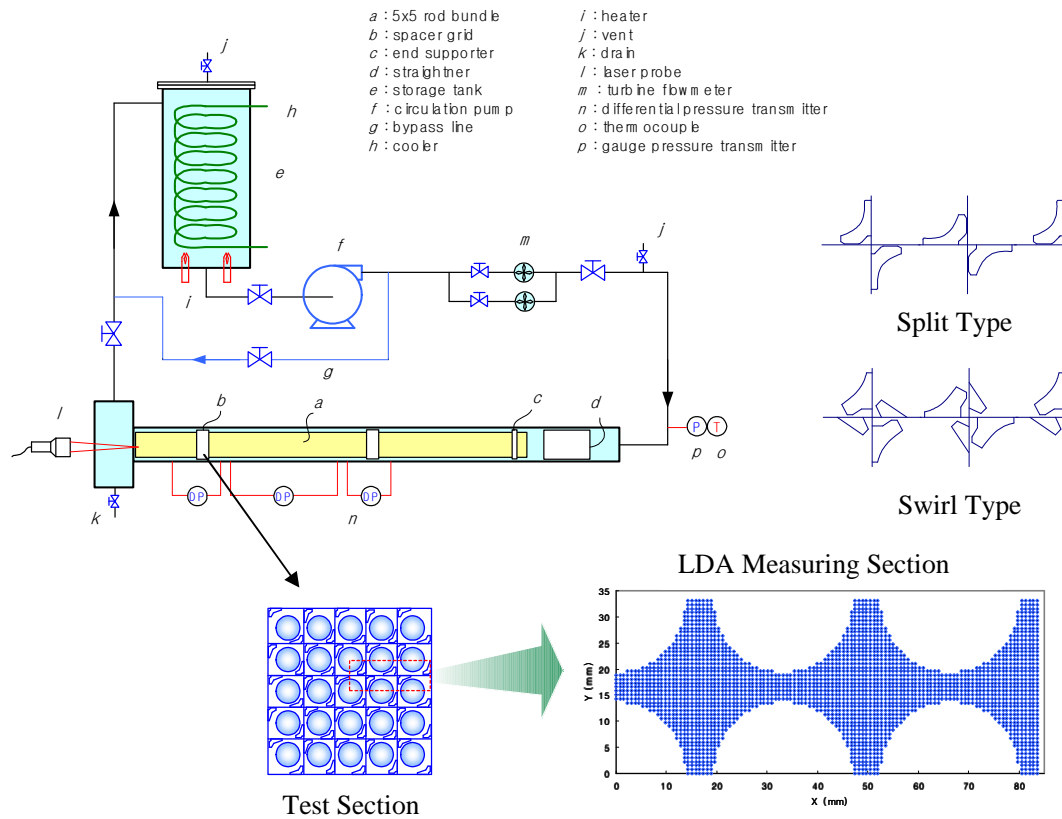
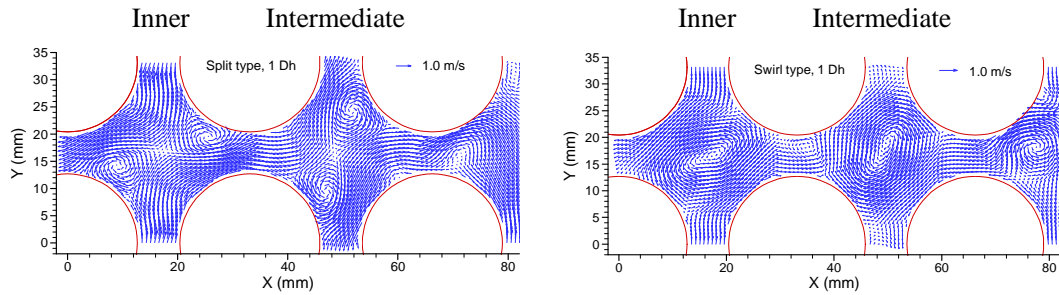


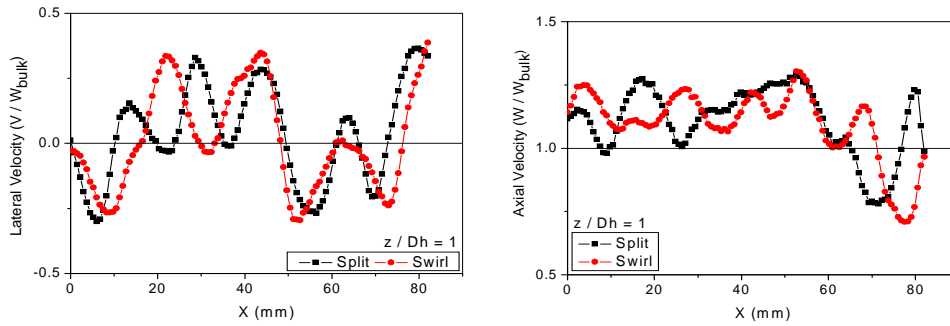
Fig. 1: MATIS-H facility (Chang et al., 2008)

According to the experimental results, as typically shown in Fig. 2, the split type of the mixing vane vigorously enhanced the flow mixing between the sub-channels through the gaps. There were a couple of symmetric vortices generated by the split vanes within a sub-channel at the inner and intermediate sub-channels. The size of each vortex is about a quarter size of the pitch. Meanwhile, the swirl type of

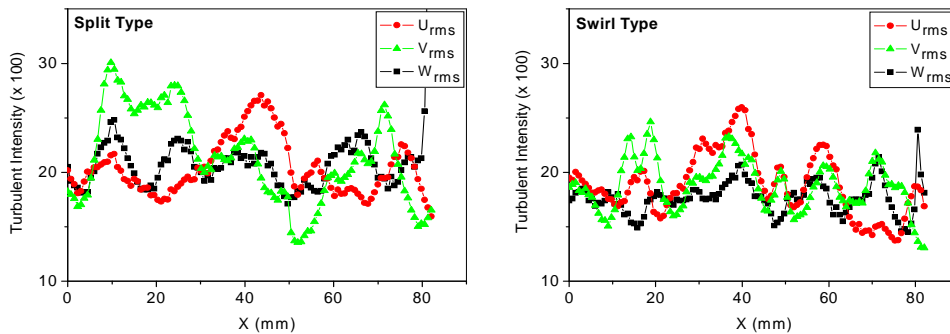
the mixing vane generated a strong vortex within a sub-channel rather than inducing the inter-subchannel flow exchanges between the sub-channels. One large vortex of elliptic shape was generated by the swirl vanes within a sub-channel at the inner and intermediate sub-channels. The size of the vortex was about 2.6 times larger than that of split type. The different patterns of vortices generation of split and swirl types affected the lateral and axial velocity profiles as shown in Fig. 2 (b). The magnitudes of the axial velocities around the vortices generated regions were about 20% lower than other region, whereas the magnitudes of the lateral velocities were about 20% higher. And also, the magnitudes of the lateral peak velocities in this investigation were about 30% of the axial bulk velocity (1.5 m/s) in both cases. The anisotropic turbulent intensity distribution were found as 16~30 % of axial bulk velocity at $z/D_h = 1$ due to the existence of the mixing vanes just upstream in both split and swirl type. These enhanced velocity fluctuations decrease gradually as the flow moved downstream, and came back to the nominal value of about 8% (Chang et al., 2008).



(a) Lateral velocity vectors at $1 D_h$ from the tip of the mixing vanes



(b) Lateral and axial velocity profiles at $1 D_h$ from the tip of the mixing vanes



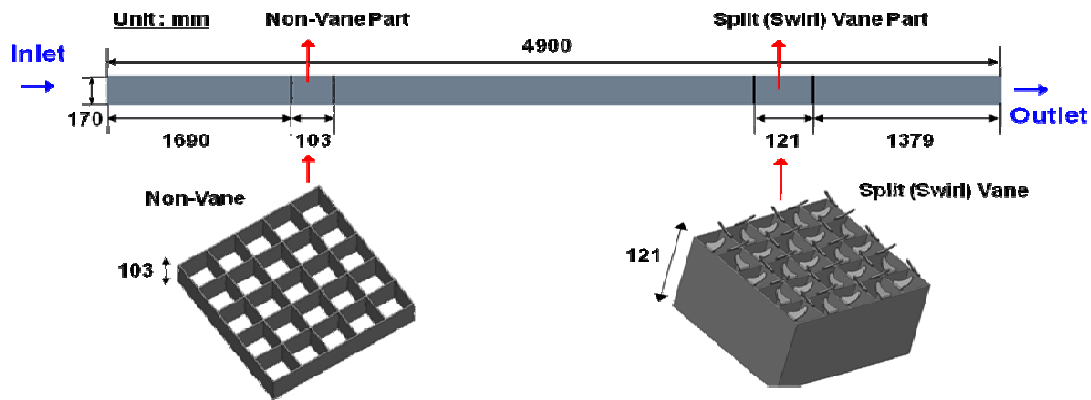
(c) Turbulent intensity values at $1 D_h$ from the tip of the mixing vanes

Fig. 2: Experimental Results of the MATIS-H (Chang et al., 2008)

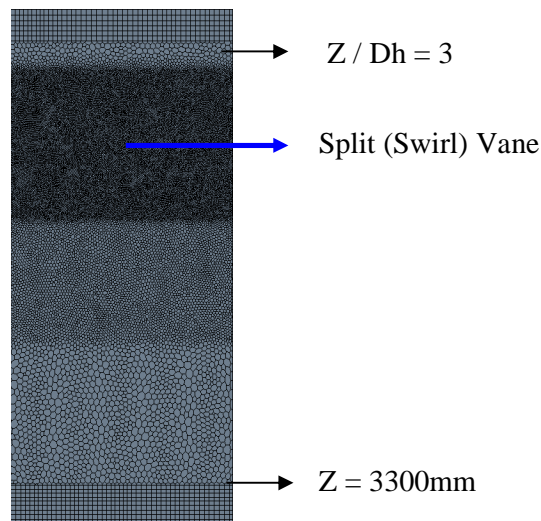
3. CFD ANALYSIS

3.1 Modeling Strategy and Grid Model

A CFD analysis was performed as one of the first step to set up the BPG for the simulation of the turbulent swirl flow due to the mixing devices in the rod bundle through a comparison work between the CFD results and the test results. A unit grid model of 5 x 5 sub-channels (Fig. 3 (a)) without an unmatched grid interface for simulating the MATIS-H facility was generated because the grid interface option in the grid model may give rise to an error in transforming CFD data between unmatched surfaces (Kang et al., 2006). A total of 10,140,474 and 10,286,576 mesh cells were produced as a base case for the split and swirl type vane, respectively. Dense mesh models for the split and swirl types were developed as shown in Table 1 to check the effect of mesh distribution at the same elevation on the flow field results in the CFD calculation. And also, a dense mesh cell distribution was located around the split and swirl vane (Fig. 3 (b)) to resolve the complicated swirl flow pattern.



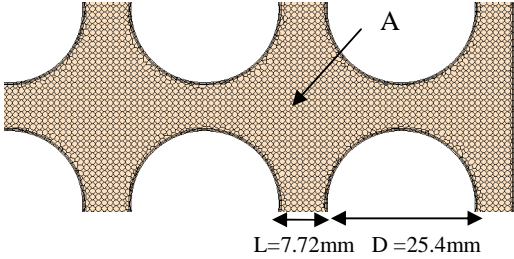
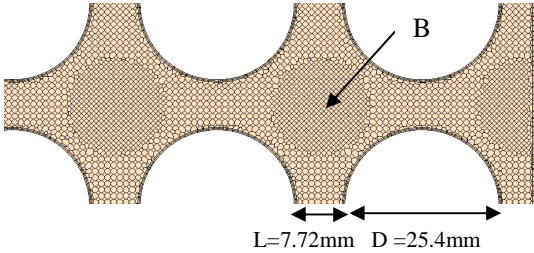
(a) Geometry outline of the grid model



(b) Mesh distribution around the mixing devices along the axial direction

Fig. 3: MATIS-H's Grid Model

Table 1 : Specification of the Grid Model-A and -B

	Split Type	Swirl Type
Model-A	Total cell number : 10,140,474 (Polyhedra+Tetra+Prism Layer)	Total cell number : 10,286,576 (Polyhedra+Tetra+Prism Layer)
	 <p>* Length of one polyhedral cell : ~ 1mm. * Mesh cell distribution on the LDA measuring section</p>	
Model-B	Total cell number : 11,297,138 (Polyhedra+Tetra+Prism Layer)	Total cell number : 11,807,599 (Polyhedra+Tetra+Prism Layer)
	 <p>* The number of mesh at the region "B" is increased about 1.5 times when compared to that of Model-A ("A")</p>	

As the first step of developing the BPG, there is a need to find which kind of CFD models can accurately predict the important features of the test results such as the velocity profile, the location of generated vortices, and turbulence characteristics due to the mixing vane type. Therefore, a series of sensitivity analysis (Table 2) was performed by varying the mesh cell distribution and the turbulent models which include the second order closures model such Reynolds Stress Models (RSM).

Table 2 : Sensitivity Calculation Conditions

	Split Type		Swirl Type	
	Turbulent Model	Grid Model	Turbulent Model	Grid Model
Case-1	Standard k-ε	Model-A	Standard k-ε	Model-A
Case-2	Reynolds Stress Model	Model-A	Reynolds Stress Model	Model-A
Case-3	Standard k-ε	Model-B	Standard k-ε	Model-B

3.2 Boundary Conditions and Governing Equations

The inlet boundary condition, the Dirichlet condition, was set at the MATIS-H's entrance region with the axial velocity of 1.5 m/s based on the test condition (Chang et al., 2008). The turbulent intensity of 5% at the inlet region was assumed. A working fluid and its operating condition were the water at 35°C and 1.4 bar. The pressure outlet boundary condition, the Neumann condition, was set for the MATIS-H's outlet (CD-adapco, 2009).

The governing equations used in this study are the mass conservation and Navier-Stokes momentum equations under the SIMPLE algorithm (CD-adapco, 2009). The turbulent flow was simulated by the standard k-ε turbulent model (Eq. (1)~(3)) and the Reynolds Stress Model (Eq. (4)~(9)) to investigate any differences of the predicted turbulence intensity between the linear and non-linear turbulent models. A standard wall function was used to treat a flow field near the wall. As for a convective numerical model, the second-order upwind difference was used. As a calculation method, 5,000~6,000 iterations were performed as a steady state until the residual of mass, enthalpy, and velocity reached below a value of 1.0E-04.

$$\frac{\partial k}{\partial t} + U_j \frac{\partial k}{\partial x_j} = P_k - \varepsilon + \frac{\partial}{\partial x_j} \left[\left(\nu + \frac{\nu_t}{\sigma_k} \right) \frac{\partial k}{\partial x_j} \right] \quad (1)$$

$$\frac{\partial \varepsilon}{\partial t} + U_j \frac{\partial \varepsilon}{\partial x_j} = C_{\varepsilon 1} \frac{\varepsilon}{k} P_k - C_{\varepsilon 2} \frac{\varepsilon^2}{k} + \frac{\partial}{\partial x_j} \left[\left(\nu + \frac{\nu_t}{\sigma_\varepsilon} \right) \frac{\partial \varepsilon}{\partial x_j} \right] \quad (2)$$

$$\nu_t = C_\mu \frac{k^2}{\varepsilon} \quad (3)$$

$$\begin{aligned} \frac{\partial}{\partial t} (\rho \overline{u_i u_j}) + \frac{\partial}{\partial x_k} (u_k \rho \overline{u_i u_j}) - \frac{\partial}{\partial x_k} \left(-\rho \overline{u_i u_j u_k} - \delta_{ik} \overline{p' u_j'} - \delta_{jk} \overline{p' u_i'} + \mu \delta_{kl} \frac{\partial}{\partial x_l} \overline{u_i u_j} \right) \\ = -\rho \left(\overline{u_i u_k} \frac{\partial u_j}{\partial x_k} + \overline{u_j u_k} \frac{\partial u_i}{\partial x_k} \right) + \Phi_{ij} - \rho \varepsilon_{ij} \end{aligned} \quad (4)$$

$$\begin{aligned} \Phi_{ij} = -\rho (C_1 \varepsilon + C_1^* P_k) b_{ij} + C_2 \rho \varepsilon \left(b_{ik} b_{kj} - \frac{1}{3} \delta_{ij} b_{kl} b_{kl} \right) + \rho (C_3 - C_3^* \Pi_b) b S_{ij}^n + \\ C_4 \rho k \left(b_{ik} S_{jk}^n + b_{jk} S_{ik}^n - \frac{2}{3} \delta_{ij} b_{kl} S_{kl}^n \right) + C_5 \rho k (b_{ik} W_{jk}^n + b_{jk} W_{ik}^n) \end{aligned} \quad (5)$$

$$C_1 = 3.4, C_1^* = 1.8, C_2 = 4.2, C_3 = 0.8, C_3^* = 1.3, C_4 = 1.25, C_5 = 0.4 \quad (6)$$

$$P_k = -\rho \overline{u_i u_j} \frac{\partial u_i}{\partial x_j} \quad (7)$$

$$b_{ij} = \frac{\overline{u_i u_j} - \frac{1}{3} \delta_{ij} \overline{u_k u_k}}{\overline{u_k u_k}} \quad (8)$$

$$\Pi_b = \sqrt{b_{ij} b_{ij}}, \quad S_{ij}^n = \frac{1}{2} S_{ij}, \quad W_{ij}^n = \frac{1}{2} \Omega_{ij} \quad (9)$$

3.3 Discussions on the CFD results

The velocity vector distribution, the axial and lateral velocity profile, and the turbulent intensity profile at $1 D_h$ and $2 D_h$ for both the split and swirl type vanes are shown in Figs 4~6. The velocity vector in Fig. 4 was defined as the absolute value of the vector. The global vector distribution and the locations of generated vortices for the split and swirl types by the CFD analysis, except the vector profile at the split type's corner sub-channel (Location-A in Fig. 4(a)), were similar to those of test data typically shown in Fig. 2 (a). But, the exact comparison between the CFD results and the test data could not be achieved because only the lateral velocity vectors were plotted in the test results whereas the lateral velocity vector could not be drawn by the STAR-CCM+ 4.02. Therefore, the comparison work of the swirl flow pattern in the sub-channel for the split and swirl types between the CFD results and the test data was done in terms of the locally axial and lateral velocity profiles along the centre line drawn from the inner to the corner sub-channel (along the lines of A-B and C-D in Fig. 5)

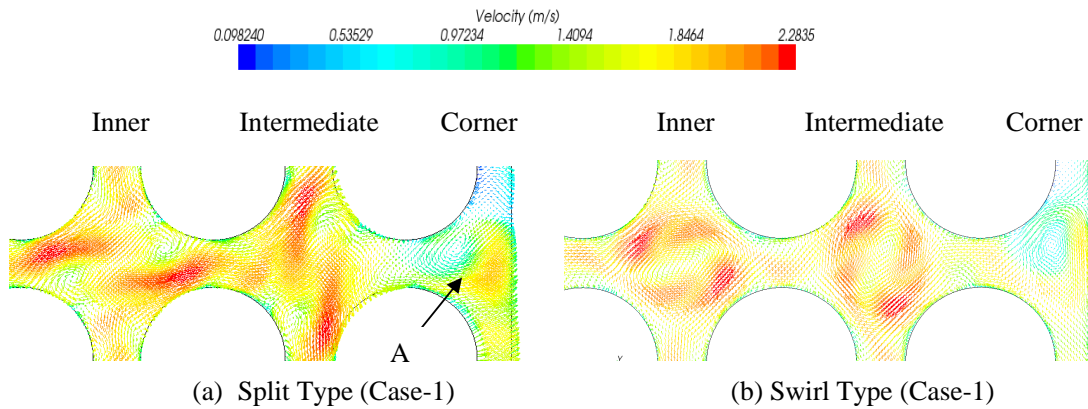


Fig. 4 : Velocity Vector Distribution in the LDA Measuring Section at $1 D_h$ by CFD Analysis

According to the comparison of the axial and lateral velocity profile at $1 D_h$ for the split and swirl vanes, the CFD results predict the test data well except the corner sub-channel region (Point-E and -F in Fig. 5). In the corner sub-channel, the predicted axial velocity values for the both vanes were about 20% lower than those of the test data. This difference may be explained by the fact that the large size swirl developed at the corner region in the CFD calculation disturbs the axial flow. This disturbance may decrease the magnitude of the axial flow velocity. And also, the velocity fluctuation along the centre line in the intermediate sub-channel of the split type was about 10~20% larger than that of test data (Point-G in Fig. 5). This may be caused by the smaller size of vortices calculated by the CFD calculation. The small vortices allowed a larger axial flow between them (Point-H in Fig. 5) in the intermediate sub-channel that induced the larger fluctuation of the axial velocity. In the swirl type, the predicted vortex size inside the intermediate sub-channel was smaller when compared to the test data. This may give rise to developing the lateral flow at the region of "I" in Fig. 5, which induces the high lateral and low axial velocity value (Point-J and -K in Fig. 5).

According to the comparison of the axial and lateral velocity profiles for the split and swirl types at $2 D_h$ between the CFD results and the test data shown in Fig. 5, the variation of the axial and lateral velocity along the centre line in the test data changed as a smooth slope, whereas those of the CFD results maintain a stiffness when compared to the values at $1 D_h$. This may mean that the vortices measured at $1 D_h$ in the test results starts to quickly decay, but the CFD calculation does not catch this swirl decay. And also, there was no big difference among the results of the Case-1, Case-2 and Case-3 in the comparison of the axial and lateral velocity profile for both split and swirl types. This may indicate that the current grid models could not resolve the detailed flow structure such as vortices' size and location and the lateral flow between the sub-channels.

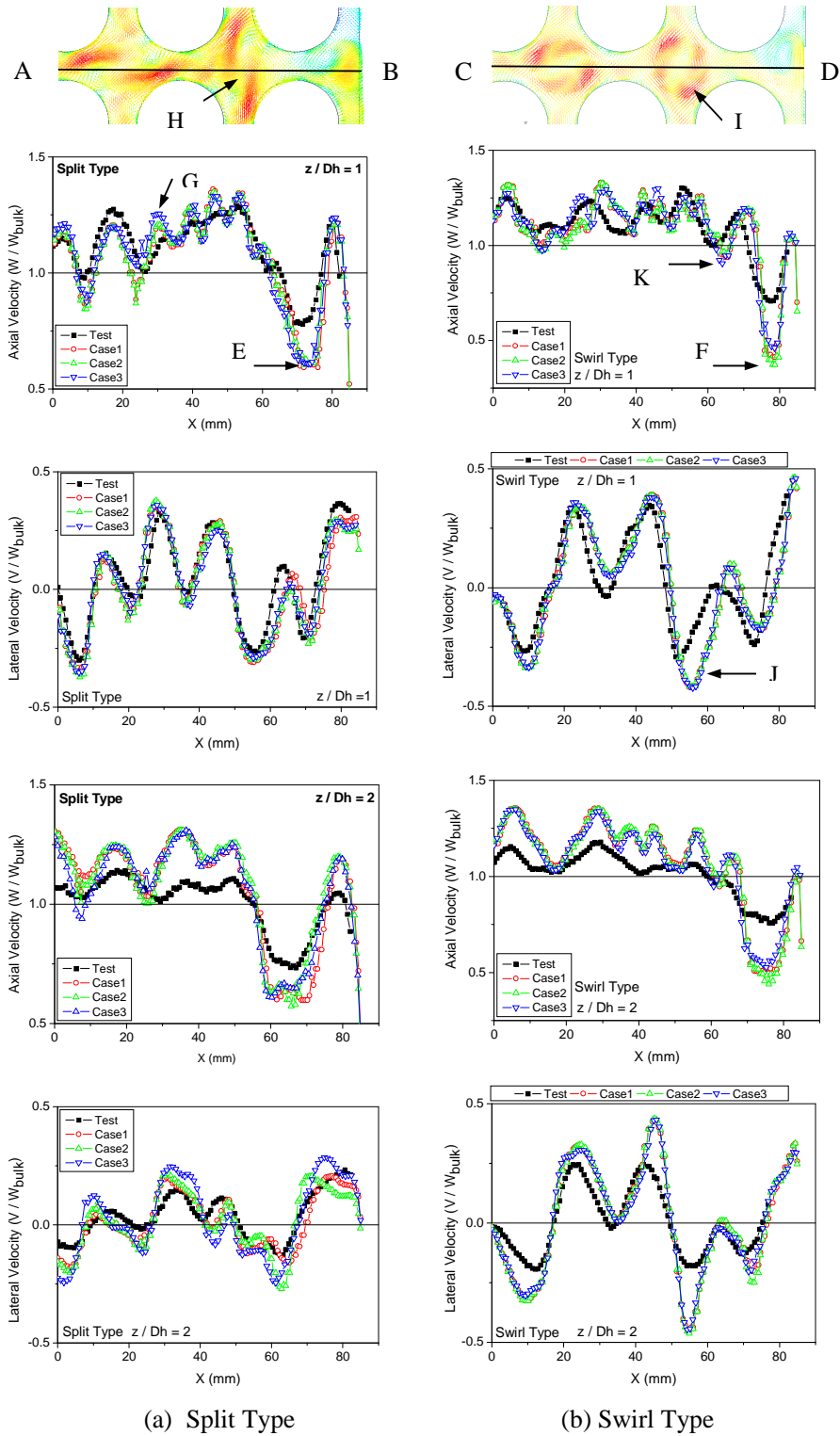


Fig. 5 : Axial and Lateral Velocity Profile along the Centre Line at 1 D_h and 2 D_h by CFD Analysis

According to the comparison of the turbulent intensity values between the test data and the CFD results for the split and swirl type shown in Fig. 6, the CFD calculation does not simulate the turbulent intensity increase up to 20~25% due to the mixing devices. This may be explained by the mesh cell distribution in the axial direction that was insufficient to resolve the drastic change of the turbulent intensity. Otherwise, the turbulent intensity of 5% at the inlet region in the CFD calculation may be a weak value when compared to the test results. Therefore, a sensitivity analysis for the turbulent intensity at the inlet region was necessary to find the reason for this difference.

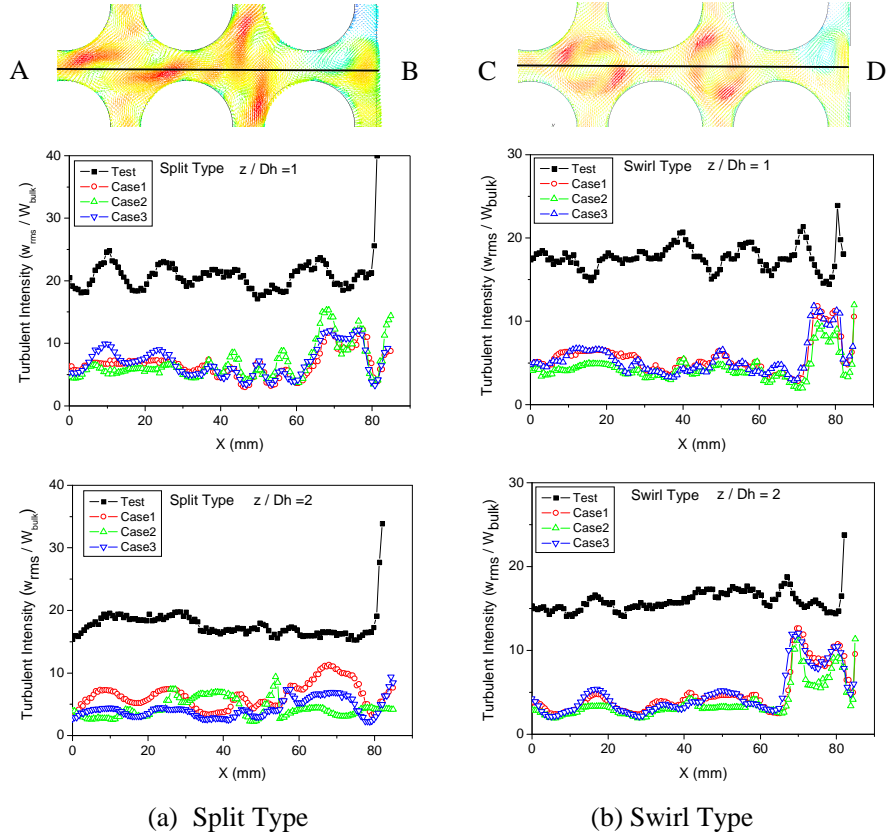


Fig. 6 : Turbulent Intensity on along Centre Line at $1 D_h$ and $2 D_h$ by CFD Analysis

4. CONCLUSIONS AND FURTHER WORK

A CFD analysis of a turbulent swirl flow developed by the typical mixing devices at the MATIS-H facility was performed using a commercial CFD code of STAR-CCM+ 4.02 with a unit grid model of 5×5 sub-channels to establish the BPG for a proper CFD analysis methodology. The CFD analysis results predicted the axial and lateral velocity profile of the test data at $1 D_h$ well, except the corner sub-channel region, but overestimated 10~20% for all sub-channels at $2 D_h$. And also, the CFD results could not predict the drastic change of turbulent intensity due to the generated vortices around the mixing devices. Therefore, a very dense mesh distribution along the axial direction around the mixing devices is recommended to accurately predict the variation of turbulent intensity. Moreover, a sensitivity analysis of the turbulent intensity at the inlet region in the CFD analysis should be performed to investigate its effect on the turbulent intensity distribution around the mixing devices. And also, we can conclude that a non-linear or second-order closure model for the turbulent flow is required to predict an anisotropic turbulent flow due to the mixing devices developed in the sub-channel.

REFERENCES

D. Bestion, "Extension of CFD Codes Application to Two-Phase Flow Safety Problems", *Nuclear Engineering & Technology*, Vol. 42, No. 4 (2010)

CD-adapco, *STAR-CCM+ Manual* (2009)

S.K. Chang, S.K. Moon, W.P. Baek, and Y.D. Choi, "Phenomenological Investigations on the Turbulent Flow Structures in a Rod Bundle Array with Mixing Devices", *Nuclear Engineering and Design*, Vol. 238, pp. 600-609 (2008)

H.S. Kang, W.K. In, and T.H. Chun, "CFD Analysis for a Turbulent Flow Field on a Hybrid 3 x 3 Channels", *Proc. Fluent Users' Conference*, Gyungju, Korea, Nov. 8-10 (2006)

H.S. Kang and C.-H. Song, "CFD Analysis for an Anisotropic Turbulent Flow Developed by a Hybrid Mixing Vane in the Fuel Assembly", *STAR-CD User Conference*, Pusan, Korea, June 2-3 (2008)

J. Mahaffy, "Development of Best Practice Guidelines for CFDE in Nuclear Reactor Safety", *Nuclear Engineering & Technology*, Vol. 42, No. 4 (2010)

J.S. Seo, *Experimental and Analytical Study on the Thermal Hydraulic Characteristics in Subchannels of 6x6 Rod Bundles with Mixing Vanes for the Safety of Nuclear Power Plant*, Ph.D. Thesis, Korea University, Korea (2009).